■ Borates |Hot Paper|

La₃B₆O₁₃(OH): The First Acentric High-Pressure Borate Displaying Edge-Sharing BO₄ Tetrahedra

The title with proper LaTeX: La$_3$B$_6$O$_{13}$(OH): The First Acentric High-Pressure Borate Displaying Edge-Sharing BO$_4$ Tetrahedra

Birgit Fuchs,[a] Gunter Heymann,[a] Xuefei Wang,[b] Abudukadi Tudi,[b] Lkhamsuren Bayarjargal,[c] Renée Siegel,[d] Adrian Schmutzler,[d] Jürgen Senker,[d] Bastian Joachim-Mrosko,[e] Andreas Saxer,[f] Zhihua Yang,[b] Shilie Pan,[b] and Hubert Huppertz*[a]

Abstract: La$_3$B$_6$O$_{13}$(OH) was obtained by a high-pressure/high-temperature experiment at 6 GPa and 1673 K. The compound crystallizes in the space group $P2_1$ (no. 4) with the lattice parameters $a = 4.785(2)$, $b = 12.880(4)$, $c = 7.433(3)$ Å, and $\beta = 90.36(10)°$, and is built up of corner- as well as edge-sharing BO$_4$ tetrahedra. It represents the first acentric high-pressure borate containing these B$_2$O$_6$ entities. The compound develops borate layers of „sechser"-rings with the La^{3+} cations positioned between the layers. Single-crystal and powder X-ray diffraction, vibrational and MAS NMR spectroscopy, second-harmonic generation (SHG) and thermoanalytical measurements, as well as computational methods were used to affirm the proposed structure and the B$_2$O$_6$ entities.

Introduction

Through the application of high pressure during a chemical reaction, astonishing new structural features in the reaction product can be accomplished. Thus, edge-sharing BO$_4$ tetrahedra were observed for the first time in 2002 by Huppertz and von der Eltz in the high-pressure borate Dy$_4$B$_6$O$_{15}$.[1] This was a remarkable discovery, because in 1960, it was postulated by Edwards, Ross,[2] and Christ,[3] that BO$_3$ groups and BO$_4$ tetrahedra can exclusively be connected through common corners. In contrast, the formation of B$_2$S$_2$, Si$_2$S$_2$, Si$_2$Se$_2$, and Si$_2$Te$_2$ rings is not unusual in the higher homologues of boron, and also in the silicon chalcogenides B$_2$S$_3$,[4–6] SiS$_2$,[7] SiSe$_2$,[7] and SiTe$_2$.[8] Reasons for their occurrence are the lower ionicity and considerably larger distances inside the four-membered rings.[1] Even

though the structural chemistry of oxoborates is in several aspects analogous to that of oxosilicates, no edge-sharing SiO$_4$ tetrahedra were found to date. One publication on „fibrous SiO$_2$" described Si$_2$O$_2$ rings forming infinite strands,[9] but these results could not be verified.

Since then, several other borates containing edge-sharing BO$_4$ tetrahedra have been discovered under high-pressure, like α-RE_2B$_4$O$_9$ ($RE=$ Y, Sm-Ho),[10–12] HP-MB$_2$O$_4$ ($M=$ Fe, Co, Ni),[13–15] HP-KB$_3$O$_5$,[16] and HP-CsB$_5$O$_8$,[17] and also under ambient and hydrothermal conditions, like in KZnB$_3$O$_6$,[18–19] Li$_4$Na$_2$CsB$_7$O$_{14}$,[20] β-CsB$_9$O$_{14}$,[21] and α-Ba$_3$[B$_{10}$O$_{17}$(OH)$_2$].[22]

For the characterization and validation of the edge-sharing BO$_4$ tetrahedra in Dy$_4$B$_6$O$_{15}$, Raman spectroscopy is an eligible method because it features two sharp bands for the B$_2$O$_6$ group in the range between ≈1200 and 1450 cm^{-1}, that is, at

[a] B. Fuchs, Prof. Dr. G. Heymann, Prof. Dr. H. Huppertz
Institut für Allgemeine, Anorganische und Theoretische Chemie
Universität Innsbruck
Innrain 80–82, 6020 Innsbruck (Austria)
E-mail: hubert.huppertz@uibk.ac.at
Homepage: http://www-c724.uibk.ac.at/aac/

[b] X. Wang, A. Tudi, Prof. Dr. Z. Yang, Prof. Dr. S. Pan
CAS Key Laboratory of Functional Materials
and Devices for Special Environment
Xinjiang Technical Institute of Physics & Chemistry, CAS
Xinjiang Key Laboratory of Electronic Information Materials and Devices
40-1 South Beijing Road, 830011 Urumqi (P. R. China)

[c] Dr. L. Bayarjargal
Institut für Geowissenschaften
Goethe-Universität Frankfurt am Main
Altenhöferallee 1, 60438 Frankfurt am Main (Germany)

[d] Dr. R. Siegel, A. Schmutzler, Prof. Dr. J. Senker
Inorganic Chemistry III and Northern Bavarian NMR Center
University of Bayreuth
Universitätsstraße 30, 95447 Bayreuth (Germany)

[e] Dr. B. Joachim-Mrosko
Institut für Mineralogie und Petrographie
Universität Innsbruck
Innrain 52, 6020 Innsbruck (Austria)

[f] Dr. A. Saxer
Institut für Konstruktion und Materialwissenschaften
Universität Innsbruck
Technikerstraße 13, 6020 Innsbruck (Austria)

Supporting information and the ORCID identification number(s) for the author(s) of this article can be found under:
https://doi.org/10.1002/chem.201905419.

Chemistry–A European Journal

Full Paper
doi.org/10.1002/chem.201905419

Chemistry Europe
European Chemical
Societies Publishing

positions where normally no signals appear in this substance class. Calculations made for HP-CsB$_5$O$_9$ confirmed the assignment of these vibrational bands to the edge-sharing BO$_4$ tetrahedra.[17] Furthermore, the possible existence of this structural feature in borate and borosilicate glasses is of great interest in the glass community and makes characterization by solid-state NMR spectroscopy inevitable. Due to the fact that most of the compounds containing edge-sharing BO$_4$ tetrahedra are paramagnetic, NMR data for this structural motif are still rare. The first NMR spectroscopic measurements were performed on HP-KB$_3$O$_5$,[16] and the ambient pressure compound KZnB$_3$O$_6$,[18–19] proving that the formation of B$_2$O$_6$ groups is not limited to extreme pressure conditions. According to the NMR data for both compounds, the authors concluded that although there are distinguishable signals, it is probably not possible to detect tetrahedra condensed to edge-sharing units on the basis of ^{11}B chemical shift data.

Moreover, the extension of structural features in borate chemistry may give rise to various new compounds with interesting properties, as oxoborates are already known for example, for their potential as materials for second-harmonic generation (SHG). The search for non-linear optical (NLO) materials in the field of borates led to various discoveries, including β-BaB$_2$O$_4$ (BBO),[23] LiB$_3$O$_5$ (LBO),[24] CsB$_3$O$_5$ (CBO),[25] CsLiB$_6$O$_{10}$ (CLBO),[26–27] and YCa$_4$O(BO$_3$)$_3$ (YCBO).[28] In the area of deep-UV NLO crystals, a breakthrough was achieved with the discovery of KBe$_2$BO$_3$F$_2$ (KBBF),[29] which represents the first material being able to generate coherent light by direct SHG at wavelengths below 200 nm. Additionally, functional layered borate materials closely related to KBBF were found to reveal a very large SHG response.[30]

In this work, we present La$_3$B$_6$O$_{13}$(OH), the first acentric high-pressure borate that features edge-sharing BO$_4$ tetrahedra. The compound was characterized by IR, Raman-, and solid-state NMR spectroscopy, to provide further data for the determination of the B$_2$O$_6$ group. Additionally, calculations and measurements of the NLO characteristics have been performed. Generally, BO$_3$ groups and cyclic 3B rings are believed to be beneficial for SHG properties due to their planar and asymmetrical shape. Despite solely consisting of corner- and edge-sharing BO$_4$ tetrahedra, La$_3$B$_6$O$_{13}$(OH) exhibits a significant SHG signal.

Results and Discussion

Crystal structure

The title compound crystallizes in the acentric space group $P2_1$ (no. 4) with the lattice parameters $a = 4.785(2)$, $b = 12.880(4)$, $c = 7.433(3)$ Å, $\beta = 90.36(10)°$ and $V = 458.13(3)$ Å^3. The crystallographic data and important refinement parameters can be found in Table 1. The positional and anisotropic displacement parameters are given in the Supporting Information in Tables S1 and S2, respectively.

The anionic framework of the structure is built up of layers in the bc plane (Figure 1). Within these layers, the BO$_4$ tetrahedra are connected by corners, as well as common edges, and develop irregular shaped „sechser"-rings. The expression

Table 1. Crystal data and structure refinement of La$_3$B$_6$O$_{13}$(OH).

Empirical formula	La$_3$B$_6$O$_{13}$(OH)
molar mass [g mol^{-1}]	706.60
crystal system	monoclinic
space group	$P2_1$ (no. 4)
single-crystal diffractometer	Bruker D8 QUEST PHOTON 100
T [K]	285(2)
radiation	Mo$_{K\alpha}$ ($\lambda = 71.07$ pm)
a [Å]	4.785(2)
b [Å]	12.880(4)
c [Å]	7.433(3)
β [°]	90.36(10)
V [Å^3]	458.13(3)
Z	2
calculated density [g cm^{-3}]	5.122
absorption coeff. [mm^{-1}]	13.837
$F(000)$	628
Crystal size [mm^3]	0.030×0.030×0.030
θ range [°]	2.74–43.31
index ranges	$-9 \leq h \leq 9$, $-24 \leq k \leq 24$, $-14 \leq l \leq 14$
reflections collected	50785
independent reflections	6882 [$R_{int} = 0.0254$]
refinement method	full-matrix least-squares on F^2
data/restraints/parameters	6882/1/214
goodness-of-fit on F^2	1.068
final $R1/wR2$ indices [$I \geq 2\sigma(I)$]	0.0162/0.0378
final $R1/wR2$ indices (all data)	0.0176/0.0383
largest diff. peak/ hole [e Å^{-3}]	2.09/−1.02
Flack parameter	0.402(2)
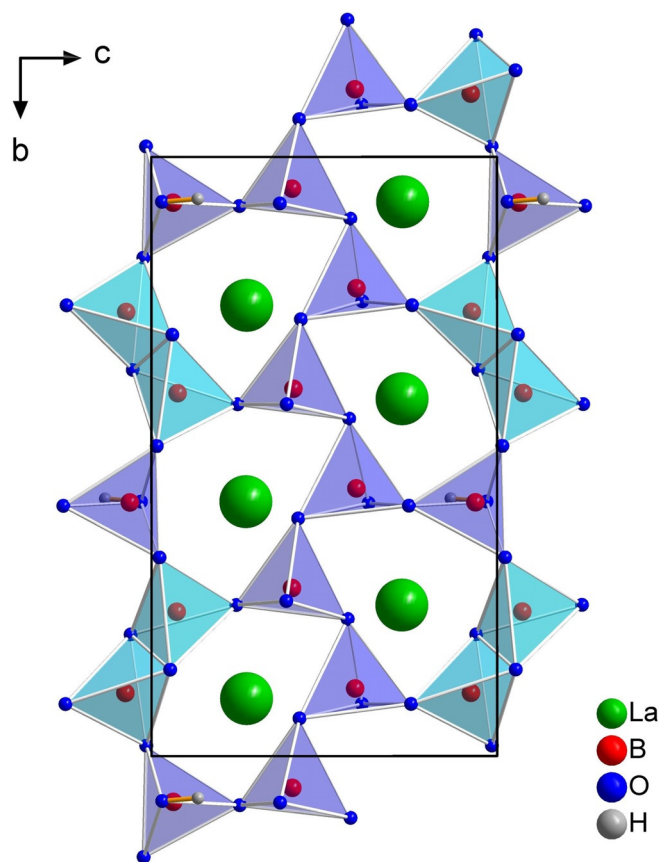
Figure 1. Crystal structure of La$_3$B$_6$O$_{13}$(OH) depicted along [$\bar{1}$ 0 0]. The corner- and edge-sharing BO$_4$ tetrahedra form layers of irregular shaped „sechser" rings.

„sechser"-ring was coined by F. Liebau, who derived the term from the German word "sechs" which means "six" for a ring with six tetrahedral centers (B).[31] There are three crystallographically different „sechser"-rings, two of them contain one B_2O_6 group each (edge-sharing BO_4 tetrahedra) and the remaining ring contains two separate halves of the B_2O_6 groups. Additionally, each ring has one hydrogen atom H1 bound to the O12 atom. These hydrogen atoms form hydrogen bonds towards the O9 atoms within the layer, as depicted in Figure 2. The corresponding bond lengths and angles are shown in Table 2.

Edge-sharing BO_4 tetrahedra are a rather rarely observed structural motif in borates. To the best of our knowledge, the presented compound is the first acentric high-pressure borate featuring this structural motif and, moreover, also the first borate, where the two boron atoms inside the edge-sharing BO_4 tetrahedra are not crystallographically equivalent. Figure 3 shows the bond lengths and angles inside the B_2O_6 dimers of $La_3B_6O_{13}(OH)$. As expected, the bond lengths inside the B_2O_2

ring (1.502–1.507 Å) are larger than those outside the ring (1.448–1.474 Å) and the O-B-O angles inside the B_2O_2 ring (92.5° and 92.7°) differ significantly from the ideal tetrahedra angle, to maximize the distance of the two central boron atoms. The B···B distance inside the edge-sharing tetrahedra of $La_3B_6O_{13}(OH)$ is 2.077 Å and, therefore, corresponds well with the values in already known high-pressure borates such as $Dy_4B_6O_{15}$ (2.072 Å), α-$Gd_2B_4O_9$ (2.04 Å), and HP-NiB_2O_4 (2.088 Å).[1,11,13] Higher B···B distances were found, for example, in HP-KB_3O_5 (2.21 Å)[16] and HP-CsB_5O_8 (2.17 Å),[17] where the oxygen atoms forming the common edge are coordinated by a third boron atom and not a metal cation, as in the aforementioned compounds with smaller B···B distances. All B–O distances and O-B-O angles can be gathered from Table 3 and Table 4.
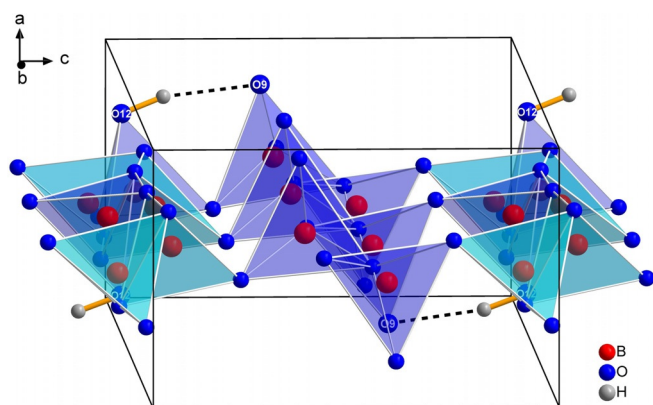

Figure 2. One layer of $La_3B_6O_{13}(OH)$ depicted along [0 1 0]. The hydrogen atoms form hydrogen bonds towards the oxygen atom O9 within the layer.

Table 2. Hydrogen bond lengths and angle for $La_3B_6O_{13}(OH)$.

Atoms	d(O–H) [Å]	d(H···O) [Å]	d(O···O) [Å]	∢(OHO) [°]
O12–H1···O9	0.83	1.78	2.59	164

Table 3. Interatomic B–O distances [Å] for $La_3B_6O_{13}(OH)$ (standard deviations in parentheses).

B1	-O1	1.459(3)	B2	-O11	1.456(4)	B3	-O7	1.450(5)
	-O4	1.469(3)		-O14	1.469(3)		-O8	1.474(5)
	-O3	1.482(3)		-O7	1.490(4)		-O6	1.502(5)
	-O2	1.509(3)		-O4	1.505(3)		-O5	1.503(5)
Ø		**1.480**	Ø		**1.48**	Ø		**1.482**
B4	-O9	1.458(3)	B5	-O10	1.466(2)	B6	-O3	1.448(5)
	-O2	1.476(3)		-O12	1.473(2)		-O13	1.470(5)
	-O10	1.487(3)		-O8	1.484(5)		-O5	1.503(5)
	-O14	1.503(3)		-O13	1.487(5)		-O6	1.507(5)
Ø		**1.481**	Ø		**1.478**	Ø		**1.482**

Table 4. Bond angles [°] for $La_3B_6O_{13}(OH)$ (standard deviations in parentheses).

O3-B1-O2	105.4(2)	O11-B2-O4	105.6(2)	O6-B3-O5	92.7(3)
O1-B1-O2	106.6(2)	O7-B2-O4	106.8(2)	O8-B3-O5	108.3(3)
O1-B1-O4	109.7(2)	O14-B2-O4	109.6(2)	O7-B3-O6	109.2(3)
O4-B1-O2	110.2(2)	O11-B2-O14	110.5(2)	O7-B3-O8	112.6(3)
O4-B1-O3	110.7(2)	O14-B2-O7	110.6(2)	O7-B3-O5	115.9(3)
O1-B1-O3	114.1(2)	O11-B2-O7	113.5(2)	O8-B3-O6	116.7(3)
Ø	**109.5**	Ø	**109.4**	Ø	**109.3**
O9-B4-O14	106.1(2)	O10-B5-O13	106.7(3)	O5-B6-O6	92.5(3)
O10-B4-O14	107.5(2)	O8-B5-O13	107.4(2)	O3-B6-O5	108.0(3)
O2-B4-O14	109.6(2)	O10-B5-O8	109.3(3)	O13-B6-O6	109.0(3)
O9-B4-O2	110.3(2)	O12-B5-O8	110.4(3)	O3-B6-O13	113.2(3)
O2-B4-O10	110.8(2)	O12-B5-O13	111.2(3)	O6-B6-O6	114.7(3)
O9-B4-O10	112.4(2)	O10-B5-O12	111.7(2)	O13-B6-O54	117.9(3)
Ø	**109.5**	Ø	**109.5**	Ø	**109.2**

Figure 3. Bond lengths and angles within the edge-sharing BO_4 tetrahedra in $La_3B_6O_{13}(OH)$.

The three crystallographically independent lanthanum cations are located between the borate layers and in the middle of the „sechser"-rings. The metal atoms La1 and La3 are ninefold coordinated by oxygen, while La2 is ten-fold coordinated (see Figure 4). The La–O distances range from 2.401 to 2.831 Å, which is in the same range as in other high-pressure lanthanum borates like γ-$La(BO_2)_3$ (2.40–3.04 Å),[32] δ-$La(BO_2)_3$ (2.45–3.10 Å),[33] and $La_2B_8O_{15}$ (2.33–2.85 Å).[34] All interatomic La–O distances are listed in Table S3.

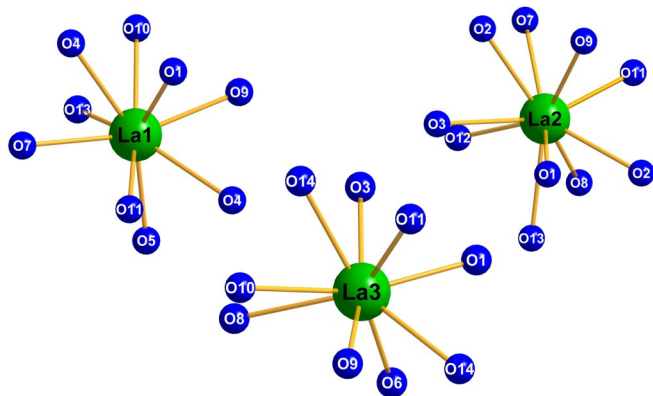Furthermore, the charge distributions were calculated according to the bond-length/bond-strength (BLBS; ΣV),[35–36] as

Chemistry–A European Journal

Full Paper
doi.org/10.1002/chem.201905419

Chemistry
Europe
European Chemical
Societies Publishing

Figure 4. Coordination of the three crystallographically independent La^{3+} cations in $La_3B_6O_{13}(OH)$.

well as the CHARDI concept (ΣQ).[37] The values obtained by both methods can be found in Table S4 and fit well to the expected formal oxidation state of $+3$ for lanthanum and boron, $+1$ for hydrogen, and -2 for oxygen. To support the position of the hydrogen atom, we also calculated the charge of the oxygen atom O12 without the bonded hydrogen atom. The unsatisfying resulting values of -1.14 and -1.18 for the two calculation methods both confirm the presented position of the hydrogen atom in the crystal structure.

CCDC 1963844 contains the supplementary crystallographic data for $La_3B_6O_{13}(OH)$. These data are provided free of charge by The Cambridge Crystallographic Data Centre through the CCDC/FIZ Karlsruhe deposition service.

X-ray powder diffraction

The comparison between the experimental and the theoretical powder pattern derived from the single-crystal structure is depicted in Figure 5. $La_3B_6O_{13}(OH)$ is clearly the major phase in the powder pattern; only very few other reflections can be

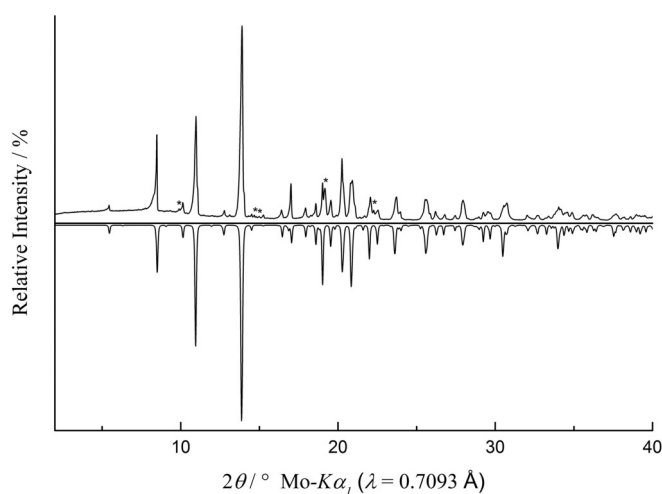**Figure 5.** Comparison of the experimental X-ray powder diffraction data $(Mo_{K\alpha_1}$ radiation, $\lambda = 0.7093$ Å; top) with the theoretical X-ray powder pattern calculated from the single-crystal data (bottom). Reflections marked with an asterisk derive from an unknown impurity.

spotted, marked with an asterisk. These additional reflections stem from a so far unknown side phase.

Electronic structure and optical properties

The calculated band gap by using GGA (Figure 6a) is 5.91 eV with an indirect characteristic. We also used the HSE06 functional to estimate a band gap of about 7.42 eV, which indicates that $La_3B_6O_{13}(OH)$ can transmit to the deep-UV region. The partial density of states (PDOS) of $La_3B_6O_{13}(OH)$ is presented in Figure 6b and shows that the valence bands (VBs) are occupied mainly by O 2p orbitals, slightly hybridized with the B 2p and H 1s orbitals. In contrast, the conduction bands (CBs) originate mainly from O 2p, B 2s2p and La 5d orbitals, while the top of the VB and the bottom of the CB are occupied mainly by O 2p, B 2p and La 5d6s orbitals.

Under the restriction of Kleinman's symmetry, $La_3B_6O_{13}(OH)$ has four independent and non-zero SHG coefficients. The calculated SHG coefficients of $La_3B_6O_{13}(OH)$ are $d_{16} = 0.998$, $d_{22} = -0.567$, $d_{23} = 0.255$, and $d_{14} = -0.00267$ pm V^{-1}. The calculated value of d_{16} is about 2.6 times that of KDP (KH_2PO_4). The band-resolved analysis for the second-order susceptibility $\chi^{(2)}$ can characterize the optical nonlinearity of crystals as shown in Figure 6b. The main response regions concentrate in the range from -5 to 0 eV in the VBs and 7.5 to 10 eV in the CBs, which is contributed by O 2p, B 2s2p, and La 5d. Therefore, the B–O and La–O groups of $La_3B_6O_{13}(OH)$ make the main contributions to the NLO properties. Moreover, the SHG density analysis[38] was used to analyse the reason for NLO-active electron states and units. Figures 6c and 6d show the SHG density of VE occupied (ve_{occ}) and unoccupied (ve_{unocc}) states. In the occupied state, B and O make the obvious contributions to the SHG effect. For the unoccupied state, La and O make main contributions for the SHG effect, but also B, O, and H. These results indicate that the La–O and B–O–H groups are the main contributors for the significant SHG response of $La_3B_6O_{13}(OH)$. Obviously, the large SHG effect in $La_3B_6O_{13}(OH)$ mainly originates synergistically from the $[B_6O_{13}(OH)]$ group and the La–O group.

The calculated birefringence of $La_3B_6O_{13}(OH)$ is 0.03 at 1064 nm as shown in Figure S1, which is attributed mainly to the structural anisotropy from covalent groups.[39]

Vibrational spectroscopy

Figure 7 shows the IR spectrum of $La_3B_6O_{13}(OH)$ between 600 and 4000 cm^{-1}. In the upper range above 3000 cm^{-1}, the expected O–H vibrations can be seen. In general, absorption bands in the region of 800 to 1200 cm^{-1} can be assigned to the tetrahedrally coordinated BO_4 group, as known for π-YBO_3, $TaBO_4$, γ-$Ln(BO_2)_3$ ($Ln = $La-Nd), and δ-$La(BO_2)_3$.[32–33,40,41] The absorption bands observed in the range between 1200 and 1500 cm^{-1} are typical for triangular BO_3 groups. Since there are no BO_3 groups in the crystal structure of $La_3B_6O_{13}(OH)$, these absorptions are related to the corresponding B-O-B, O-B-O, and B-O-La vibrations, which has been verified for the oxoborates β-ZnB_4O_7 and β-CaB_4O_7 by ab initio quantum chemical calculations.[42]

Chemistry–A European Journal | Full Paper
doi.org/10.1002/chem.201905419

Chemistry
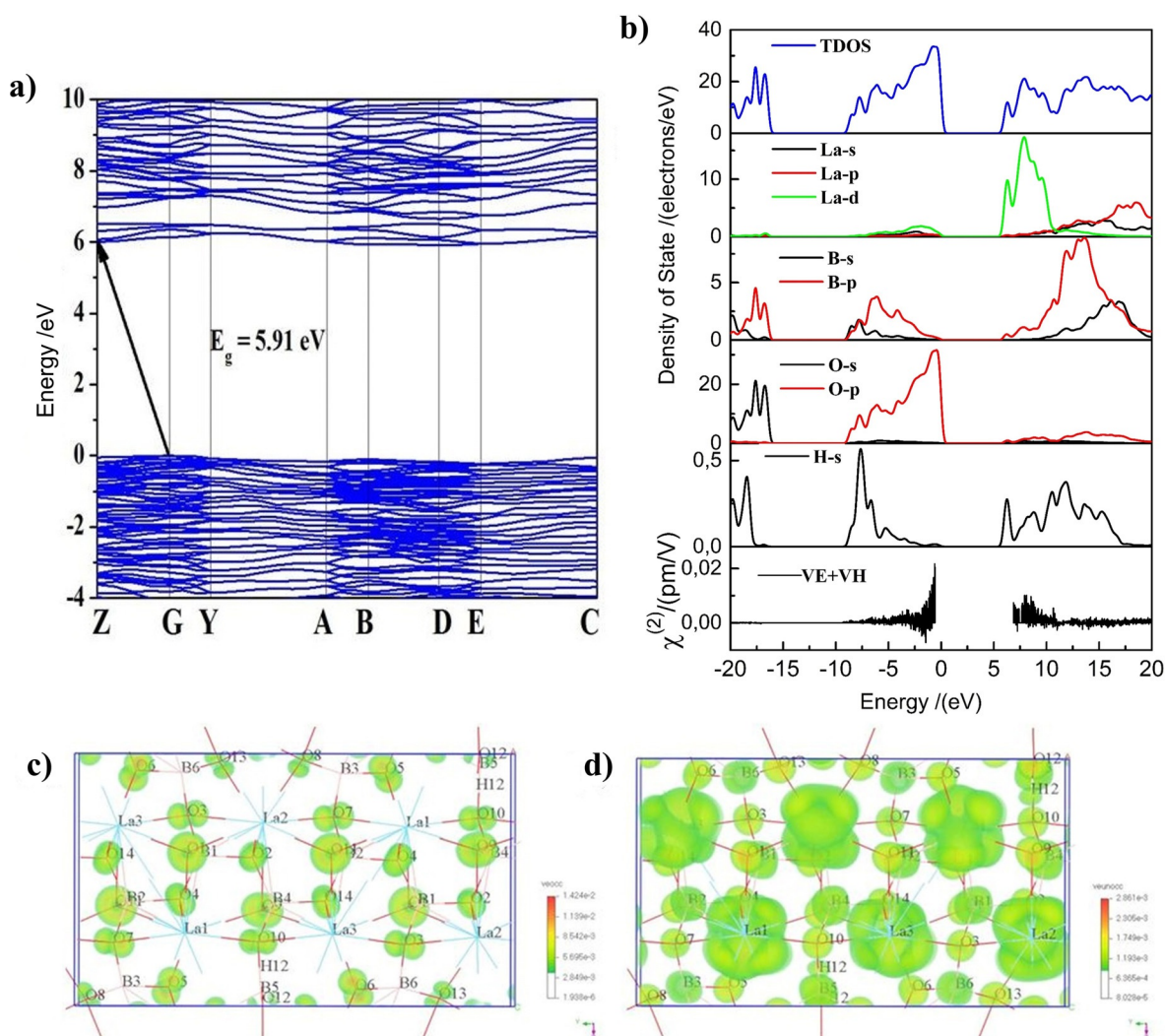Europe
European Chemical
Societies Publishing

Figure 6. a) Electronic band structure; b) partial density of states and band-resolved analysis of SHG; SHG density maps of the c) VE occupied and d) VE unoccupied orbitals.
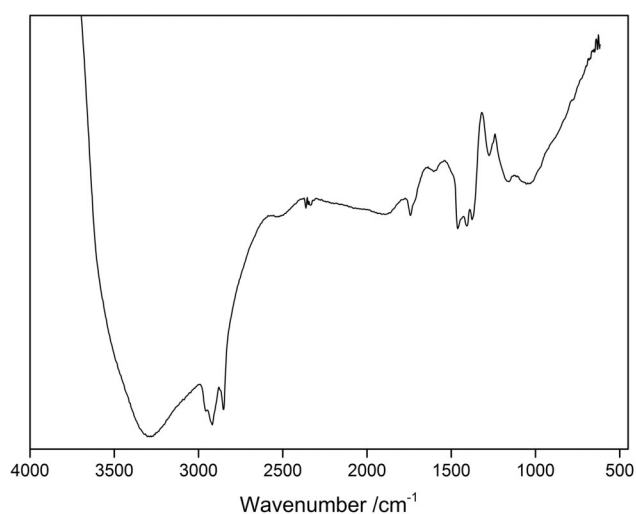

Figure 7. IR spectrum of a $La_3B_6O_{13}(OH)$ single-crystal.

The spikes at 2800–2950 cm^{-1} and at 1700 cm^{-1} stem from the oil which was used to prepare the crystals.

The single-crystal Raman spectrum of $La_3B_6O_{13}(OH)$ is shown in Figure 8 in the range of 200 to 1600 cm^{-1}. The two sharpest bands in the spectrum are located at $\tilde{v}=1295$ and 1438 cm^{-1}. Normally, this range corresponds to the stretching vibrations of BO_3 or OB_3 groups. Since the investigated compound does not contain trigonal coordinated boron or threefold-coordinated oxygen atoms, these peaks are assumed to be the Raman-active modes of the B_2O_6 unit of the edge-sharing BO_4 tetrahedra. Similar bands were found in the Raman spectra of other compounds featuring edge-sharing BO_4 tetrahedra, for example in $Dy_4B_6O_{15}$ (1271 and 1435 cm^{-1}), α-$Gd_2B_4O_9$ (1253 and 1431 cm^{-1}), and HP-NiB_2O_4 (1262 and 1444 cm^{-1}).[1,11,13] In contrast to that, the high-pressure borate HP-KB_3O_5 and the compound $KZnB_3O_6$, which was synthesized under ambient conditions, exhibit only one signal for the edge-sharing BO_4 tetrahedra and miss the vibrational band at around 1400 cm^{-1}. This difference to the previously discussed compounds originates
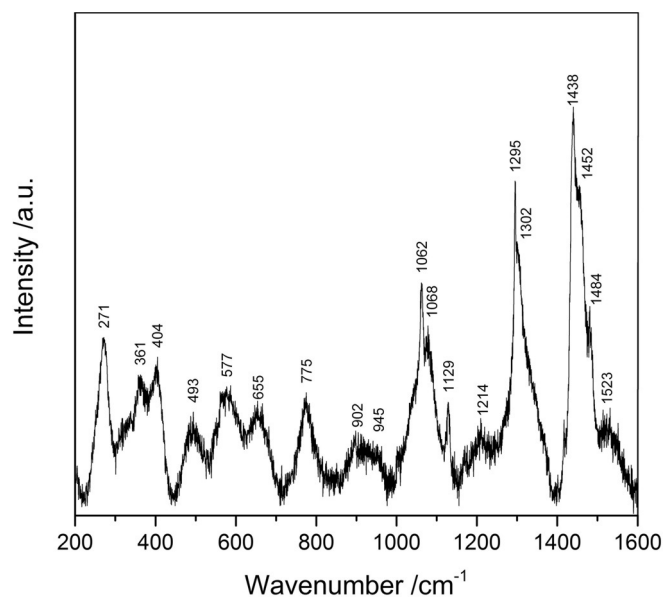
Figure 8. Raman spectrum of a $La_3B_6O_{13}(OH)$ single-crystal.

presumably in the increased boron coordination of the oxygen atoms forming the common edge of the B_2O_6 unit.[16,18]

Vibrational bands in the range of 620–1200 cm^{-1} can be assigned to the BO_4 stretching vibrations, while BO_4 bending vibrations can be seen at $\tilde{v} < 900$ cm^{-1}. Below $\tilde{v} = 400$ cm^{-1}, the La–O stretching modes occur, as well as complex lattice vibrations.[43]

Second-harmonic generation measurements

The SHG properties of the $La_3B_6O_{13}(OH)$ sample were investigated with the powder SHG method developed by Kurtz and Perry.[44] This method is commonly used as a first step to estimate the NLO properties of new materials or to detect the absence of an inversion center in crystalline structures.

Table 5 shows the intensity of the SHG signal of the sample in comparison to several reference compounds (α-Al_2O_3, Quartz, KDP). The ratio of the sample signal and the reference signal of quartz provides an estimation of the effective SHG coefficient.

The recommended standard values of references are $d_{11} = 0.30$ pm V^{-1} for the quartz and $d_{14} = 0.39$ pm V^{-1} for KDP at 1064 nm.[45] Although both reference crystals (KDP and quartz) have comparable SHG coefficients, phase matching of KDP provides one order higher SHG signals than non-phase matchable crystals such as quartz. In the case of phase match-

ing, we are expecting the same order of SHG intensities like KDP for $La_3B_6O_{13}(OH)$. However, the SHG intensity of $La_3B_6O_{13}(OH)$ yielded around 20 mV, which is $\approx 2/3$ the intensity of quartz. On the basis of calculated SHG coefficients and the measured SHG signal we can suppose that $La_3B_6O_{13}(OH)$ is a non-phase matchable crystal. Additionally, the relatively large Flack parameter of 0.402, determined in the structure analysis, can also be related to the considerably reduced SHG response in contrast to the calculated SHG coefficients. Nevertheless, the notable SHG signal indicates that the sample $La_3B_6O_{13}(OH)$ clearly crystallizes in a non-centrosymmetric space group. The SHG intensities of $La_3B_6O_{13}(OH)$ have a very large standard deviation due to large intensity differences from different area. One possible reason for the difference between calculated and measured SHG values can be the difference between grain sizes of the sample and references. Grain size dependence of SHG signals was not carried out here.

Solid-state NMR spectroscopy

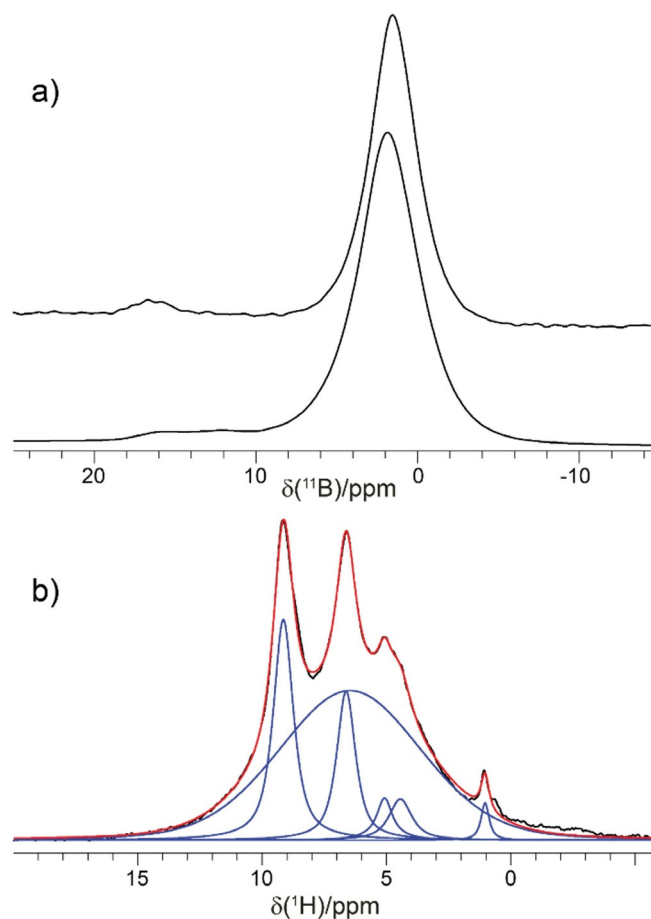The ^{11}B and ^{1}H MAS NMR spectra recorded for $La_3B_6O_{13}(OH)$ powders are depicted in Figures 9a and 9b. The ^{11}B NMR spec-

Figure 9. a) ^{11}B MAS NMR spectra of $La_3B_6O_{13}(OH)$ at 1.0 GHz (top) and 600 MHz (bottom) recorded with spinning speeds of 40 and 20 kHz, respectively. b) ^{1}H MAS NMR spectrum (black) at 600 MHz and a spinning speed of 62.5 kHz along with a deconvolution (blue) and resulting line shape (red).

Table 5. SHG intensity of a $La_3B_6O_{13}(OH)$ powder sample compared with the three reference materials.

Compound	SHG Intensity [mV]	$I_{SHG}/I_{Quartz}*100\%$
α-Al_2O_3	0.2 (0.2)	0.6
Quartz	31.0 (9.9)	100
KDP (KH_2PO_4)	296.9 (31.1)	958
$La_3B_6O_{13}(OH)$	19.7 (17.6)	63

Chemistry–A European Journal

Full Paper
doi.org/10.1002/chem.201905419

Chemistry Europe
European Chemical
Societies Publishing

trum shows two peaks at about 2 and 17 ppm. The peak at 17 ppm exhibits the typical second-order quadrupolar shape, which is more pronounced for the 600 MHz spectrometer and narrows for the spectrum collected on the 1.0 GHz instrument, as this interaction scales inversely with the external magnetic field. Its quadrupolar coupling constant, C_Q, is estimated to be about 2.4 MHz with an asymmetry close to 0. This C_Q and isotropic shift are typical for trigonal BO_3[16,46] and since this peak's intensity is small (less than 5%), we assign it to an impurity containing trigonal BO_3 units. The main peak at 2 ppm, together with its significantly smaller second-order quadrupolar broadening, is typical for BO_4 tetrahedral groups. The spectral resolution, even for the 1.0 GHz spectrometer, is not sufficient to resolve the expected six crystallographically inequivalent boron sites. Lineshape analyses of the first-order satellites (Figure S2) suggest C_Q values smaller than 500 kHz for all BO_4 units. This is in line with quantum mechanical calculations on the DFT level (Table S5), where predicted isotropic chemical shifts differ only by 0.5 ppm and the C_Q values are between 200 and 500 kHz.

In contrast to the expected single resonance for the OH group within $La_3B_6O_{13}(OH)$, the ^1H MAS NMR spectrum (Figure 9 b) shows a surprisingly rich spectral signature with two main sharp resonances at 9.2 and 6.6 ppm. Additionally, one broad signal at 6.5 ppm, typical for an amorphous side phase, and three weak peaks at 1.0, 4.5, and 5.1 ppm were observed. To derive connectivities, 2D ^1H-^{11}B HETCOR (Figure 10) and ^1H-^1H DQ-SQ correlation (Figure S3) NMR spectra were recorded. Only ^1H NMR signals at 9.2, 6.6, and 6.5 ppm are correlated to ^{11}B NMR resonances, rendering all other proton resonances (1.0, 4.5, and 5.1 ppm) to signals originating from boron-free impurities. While the amorphous side phase at 6.5 ppm mostly consists of BO_4 units, the resonance at 6.6 ppm correlates with
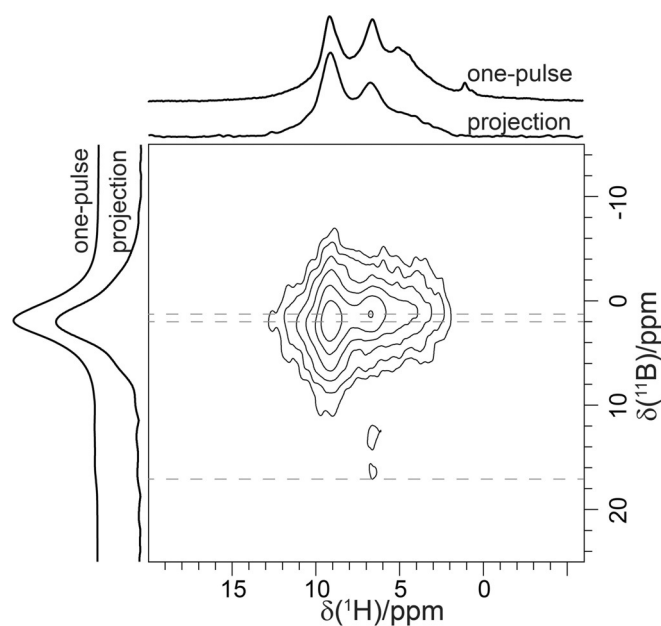
both BO_4 and BO_3 species. Since $La_3B_6O_{13}(OH)$ does not contain any BO_3, this peak is also assigned to impurities. This leaves the resonance at 9.2 ppm for the OH group present in the structure. The assignment is corroborated by the ^1H-^1H DQ-SQ spectrum (Figure S3), which shows that almost all the resonances exhibit self-correlations only. This is characteristic for ^1H signals originating from different phases. In line with the low proton density for $La_3B_6O_{13}(OH)$, the self-correlation for the resonance at 9.2 ppm is weak. The significantly higher intensities for the other self-correlations suggest a higher proton density for the impurities and the amorphous side phase. Without actual knowledge about the proton densities of the side phases, an estimate of their content is not possible from the NMR data.

To conclude, the ^{11}B and ^1H NMR results are in agreement with the proposed structure model obtained from XRD, but indicate the presence of both amorphous and crystalline impurities. The relatively high shift of 9.2 ppm for the protons of the OH units confirms a medium strong hydrogen bond interaction to neighboring oxygen atoms.

Thermal behavior

To study the high-temperature stability, thermoanalytical measurements of $La_3B_6O_{13}(OH)$ were performed. Figure 11 depicts the results from the thermogravimetric (TG), the differentiated thermogravimetric (DTG) analyses, and the differential thermal analysis (DTA) recorded from room temperature to 970 °C. Until approximately 150 °C, a mass increase can be observed. This most likely results from the small initial weight and consequential correction effects. $La_3B_6O_{13}(OH)$ is stable up to 708.2 °C, visible as an endothermic peak in the DTG curve. This is in good agreement with the HT-XRD data (see Figure 12), where the slow decomposition of the compound starts around 710–720 °C. Furthermore, additional reflections appear in the powder patterns above this temperature, which can be as-
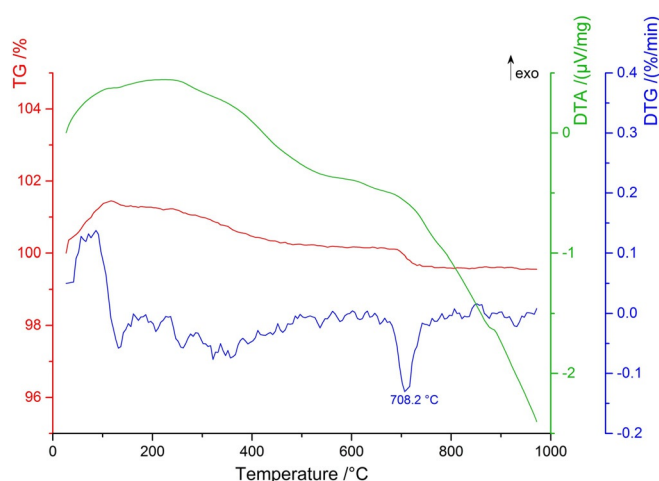
Figure 10. 2D ^1H–^{11}B *D*-HMQC correlation spectrum at 600 MHz. The spinning speed was adjusted to 62.5 kHz.

Figure 11. The simultaneous thermal analysis (STA) of $La_3B_6O_{13}(OH)$ with the thermogravimetric (TG) curve in red, the differentiated thermogravimetric (DTG) curve in blue, and the differential thermal analysis (DTA) curve in green.
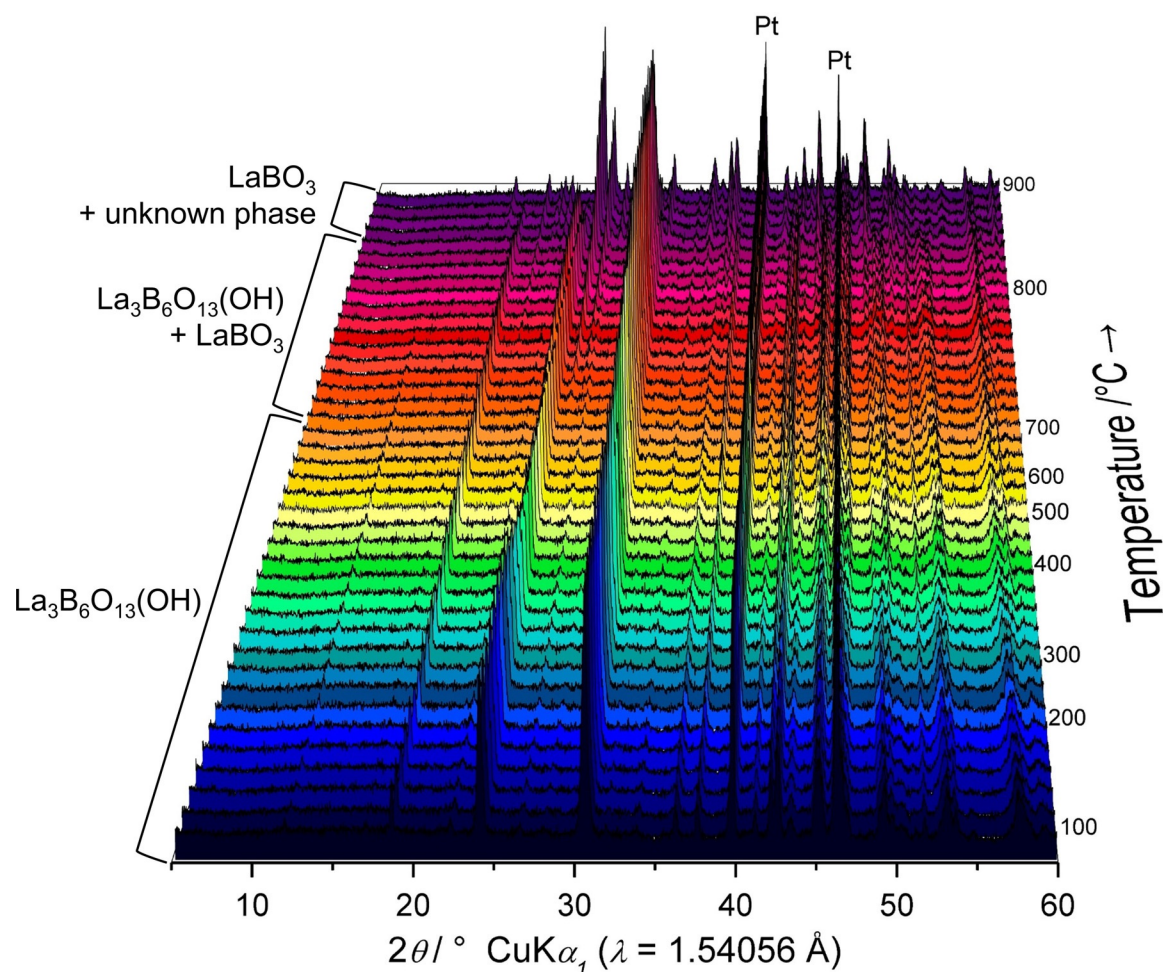
Chemistry–A European Journal

Full Paper
doi.org/10.1002/chem.201905419

Chemistry
Europe
European Chemical
Societies Publishing

Figure 12. HT-XRD of $La_3B_6O_{13}(OH)$ with representation of the range the respective compound occurs. $La_3B_6O_{13}(OH)$ decomposes starting from about 720 °C up to 850 °C. After this temperature, λ-$LaBO_3$ and at least one additional unknown phase is present. The platinum reflections stem from the heating band.

signed to λ-$LaBO_3$. At approximately 850 °C, $La_3B_6O_{13}(OH)$ decomposes completely and only λ-$LaBO_3$ as the main phase, besides another unknown compound, is visible.

Conclusions

$La_3B_6O_{13}(OH)$ represents the first acentric high-pressure borate containing edge-sharing BO_4 tetrahedra and, to the best of our knowledge, the first borate, where the two boron atoms inside these tetrahedra are not crystallographically equivalent. The anionic borate backbone builds up layers of „sechser"-rings in the bc plane. The lanthanum cations are located between the layers and in the middle of the „sechser"-rings.

The SHG measurements of $La_3B_6O_{13}(OH)$ yielded a significant signal and confirmed the acentric space group from the single-crystal structure determination. Additional calculations, ^{11}B MAS NMR investigations, and the results from the vibrational spectroscopy also support the described crystal structure and the existence of the structural motif of edge-sharing BO_4 tetrahedra.

Experimental Section

Synthesis: For the synthesis of $La_3B_6O_{13}(OH)$, a homogeneous mixture of La_2O_3 (Strem Chemicals, Newburyport, USA, 99.9%) and H_3BO_3 (Carl Roth, Karlsruhe, Germany, >99.8%) in the stoichiometric ratio of 1:4 was filled into a Pt-capsule, placed into a crucible made of α-BN and closed with a lid (also α-BN; Henze Boron Nitride Products AG, Germany). The compression and heating were carried out in a Walker-type multianvil module combined with a 1000 t hydraulic press (both Max Voggenreiter GmbH, Germany). The 18/11 assembly was compressed in a two-step mechanism by six steel wedges (outer anvils) and by eight tungsten carbide cubes (inner anvils; Hawedia, Marklkofen, Germany). A detailed description of this setup can be found in the literature.[47–49]

The assembly was compressed to 6 GPa in 150 minutes and heated to 1673 K in the following 10 minutes. The temperature was kept for 10 minutes, before the heating was switched off to quench the sample to room temperature. Afterwards, the 450 minute decompression process started. The product was separated mechanically from the surrounding platinum foil and the microcrystalline colorless $La_3B_6O_{13}(OH)$ was recovered.

To receive single-crystal platelets, the sample had to be compressed to higher pressures above 12 GPa and slowly cooled down to 773 K in two to three hours. Using this scheme, measurable

Chemistry–A European Journal

Full Paper
doi.org/10.1002/chem.201905419

Chemistry Europe
European Chemical
Societies Publishing

single crystals could be received. Unfortunately, the received product was not phase pure and the unknown side phases could not be quantified.

Single-crystal structure analysis: The single-crystal intensity data were collected at 213 K with a Bruker D8 Quest Kappa diffractometer equipped with a Photon 100 CMOS detector. Monochromatized Mo$_{K\alpha}$ radiation ($\lambda = 0.7107$ Å) was generated with an Incoatec microfocus X-ray tube and a multilayer optic. A multiscan absorption correction of the intensity data was performed with SADABS 2014/5,[50] and for the structure solution and parameter refinement, the SHELXS/L-2013[51–52] software implemented in WINGX-2013.3[53] was used. During the refinement, the acentric space group $P2_1$ (no. 4) was found to be correct after initial attempts to solve the structure in the higher symmetric space group $P2_1/m$ (no. 11). To emphasize the regularity of the structure solution, the ADDSYM routine of the program PLATON[54] was performed, which found no additional symmetry operations within the final structure solution. With a Flack parameter of 0.402 the crystal was refined as a two-component inversion twin. All non-hydrogen atoms were refined with anisotropic displacement parameters. The final positional parameters were standardized employing STRUCTURE TIDY,[55] as implemented in PLATON.

X-ray powder diffraction: The microcrystalline sample of La$_3$B$_6$O$_{13}$(OH) was analyzed on a Stoe Stadi P powder diffractometer (STOE & Cie GmbH, Darmstadt, Germany) in transmission geometry with Ge(111)-monochromatized Mo$_{K\alpha1}$ radiation ($\lambda = 70.93$ pm). The reflections were detected with a Dectris MYTHEN 1 K microstrip detector. The measurement was performed in the 2θ range of 2–52° with a step size of 0.015°.

Computational methods: The density functional theory (DFT) was used to study the electronic structure and optical properties of La$_3$B$_6$O$_{13}$(OH).[56] The generalized gradient approximation (GGA)[57] with Perdew–Burke–Ernzerhof (PBE)[58] functional and norm-conserving pseudopotentials (NCP) were applied under the geometry optimization. A plane-wave cutoff energy of 750 eV and the Monkhorst–Pack k-point mesh ($6 \times 2 \times 4$) were chosen to achieve a well converged electronic structure and optical properties. Moreover, NLO coefficients at a zero frequency were calculated by using a formalism developed by Aversa and Sipe.[57] At a zero frequency, the formula of second-order NLO coefficients can be derived as Eq. (1–3):[60]

$$\chi^{\alpha\beta\gamma} = \chi^{\alpha\beta\gamma}(VE) + \chi^{\alpha\beta\gamma}(VH) \tag{1}$$

$$\chi^{\alpha\beta\gamma}(VH) = \frac{e^3}{2\hbar^2 m^3} \sum_{vv'c} \int \frac{d^3k}{4\pi^3} P(\alpha\beta\gamma) \mathrm{Im}[p^\alpha_{vv'} p^\beta_{v'c} p^\gamma_{cv}]\left(\frac{1}{\omega^3_{cv}\omega^2_{v'c}} + \frac{2}{\omega^4_{vc}\omega_{cv'}}\right) \tag{2}$$

$$\chi^{\alpha\beta\gamma}(VE) = \frac{e^3}{2\hbar^2 m^3} \sum_{vcc'} \int \frac{d^3k}{4\pi^3} P(\alpha\beta\gamma) \mathrm{Im}[p^\alpha_{vc} p^\beta_{cc'} p^\gamma_{c'v}]\left(\frac{1}{\omega^3_{cv}\omega^2_{vc'}} + \frac{2}{\omega^4_{vc}\omega_{c'v}}\right) \tag{3}$$

Here, α, β, γ are Cartesian components, v and v' represent valence bands, c and c' represent conduction bands. P($\alpha\beta\gamma$) represents the full permutation, and $\hbar\omega_{ij}$ and P_{ij}^α represent the band energy difference and the momentum matrix elements, respectively.

Quantum-chemical calculations for the solid-state NMR spectroscopy were also performed using the plain-wave density functional theory (DFT) program CASTEP[56] version 17.2.

Based on the structure solution, a geometry optimization with a cutoff energy of 1200 eV was performed. The optimization used

the Broyden–Fletcher–Goldfarb–Shanno (BFGS) algorithm.[61–64] K-Points were determined by a Monkhorst–Pack grid,[65] with a maximum distance of 0.07 Å^{-1}, resulting in 6 k-points for the calculations. For the geometry-optimized structure, the same parameters were used to calculate tensors of the chemical shielding and the quadrupolar interaction using the GIPAW approach.[66]

Vibrational spectroscopy: The single-crystal absorption spectrum of La$_3$B$_6$O$_{13}$(OH) was acquired using a Bruker Vertex 70 FT-IR spectrometer (spectral resolution 4 cm^{-1}) equipped with KBr beam splitter, a mercury cadmium telluride (MCT) detector and a coupled Bruker Hyperion 3000 microscope. The single-crystal was placed on a BaF$_2$ carrier and measured in transmittance mode in the spectral range 600–4000 cm^{-1}. A Globar mid-IR source was used as well as a $15\times$ IR objective. 320 scans of the sample were recorded and corrected for atmospheric effects with the OPUS 6.5 software.[67]

The Raman spectrum of a La$_3$B$_6$O$_{13}$(OH) single-crystal was measured using a Horiba Jobin Yvon LabRam HR-800 microspectrometer. The excitation of the sample was accomplished with a 532 nm frequency-doubled 100 mW neodymium-doped yttrium aluminum garnet (Nd:YAG) laser that was focused on the sample surface with an Olympus 50× objective lens. An optical grating with 1800 lines mm^{-1} was used to disperse the scattered light, which was then collected by a cooled Andor CCD detector with 1024× 256 pixels. Three spectra with an acquisition time of 40 s each were analyzed in the 200–1600 cm^{-1} Raman shift range in multiwindow acquisition mode and averaged with the LABSPEC software (version 5.93.20).[68] The spectra were recorded at ambient conditions and the background was corrected with an eighth-order polynomial line-segment function.

Second-harmonic generation measurements: Second-harmonic generation (SHG) measurements were performed on a powder sample of La$_3$B$_6$O$_{13}$(OH). A Q-switched Nd:YAG laser (1064 nm, 5–6 ns, 2 kHz) was used for the generation of the fundamental pump wave. With a harmonic separator, a short-pass filter and an interference filter, the fundamental infrared light was separated from the generated second harmonic (532 nm). The generated SHG signal was collected on eleven different areas of the sample to check its homogeneity. On each position 64 pulses were measured and averaged. The measured intensities were background-corrected by signals collected between the laser pulses. As reference materials α-Al$_2$O$_3$, quartz and KDP (KH$_2$PO$_4$) were used.

A detailed description of the experimental setup for the powder SHG measurement is given by Bayarjargal et al.[69]

Solid-state NMR spectroscopy: ^{11}B MAS NMR spectroscopic experiments were measured on Bruker Avance III HD spectrometers at B_0 fields of 14.1 T (600 MHz) and 23.4 T (1.0 GHz) corresponding to ^{11}B Larmor frequencies of 192.6 and 320.9 MHz, respectively. The samples were spun at 20–62.5 kHz in a 1.3 mm MAS double resonance probe (Bruker). The ^{11}B NMR spectrum was acquired by single pulse excitation with a pulse of 1.0 μs having a small flip angle of about 10° and with a recycle delay of 1.0 s. The spectra are referenced to boron trifluoride etherate (BF$_3$·Et$_2$O) using NaBH$_4$ as a secondary reference (−42.06 ppm).[70] The ^{1}H MAS NMR spectrum was recorded at a ^{1}H frequency of 600.1 MHz, with a spinning of 62.5 kHz, a 90° pulse of 1.4 μs and with a recycle delay of 300 s. The ^{1}H-^{11}B HETCOR NMR spectrum was acquired at a B_0 field 14.1 T, with a MAS of 62.5 kHz using the D-HMQC sequence[71–72] with a SR4 recoupling[73] of 256 μs. Finally, the ^{1}H-^{1}H DQ-SQ experiment was obtained at a ^{1}H frequency of 600.1 MHz, with a spinning of 62.5 kHz and using the symmetry-based R12$_2^5$ recoupling[74] with each R element being a 180° pulse and with a total DQ excitation/reconversion time of 64.0 μs.

Thermoanalytical investigations: The simultaneous thermal analysis (STA) of the $La_3B_6O_{13}(OH)$ sample was carried out on a NETZSCH STA 449 F5 instrument. This enables the differential thermal analysis (DTA) to be performed simultaneously with a thermogravimetric analysis (TGA). Sample weight, mass increase/decrease, and thermal information can be provided continuously throughout the heating process. A difference in the heat flow (DTA) between the sample and the reference is detected as an exothermic or endothermic signal inside the sample. 10.66 mg of the sample were weighed into an Al_2O_3 crucible and heated from 25 °C to 1000 °C under air with a heating rate of 10 °C min^{-1}.

High temperature XRD: A PANALYTICAL Empyrean powder diffractometer in theta–theta geometry was employed to collect the high-temperature X-ray diffraction patterns of $La_3B_6O_{13}(OH)$. The diffractometer is equipped with a Cu tube (tension: 40 kV; current: 40 kV) and a PIXCEL 1D detector. Furthermore, a variable divergence slit with an irradiated length of 6 mm was used. The powder sample was applied on a platinum strip (thickness: 1 mm) and measured under air in an Anton Paar HTK 16N high temperature strip-heater chamber in the temperature range from 25 °C to 900 °C.

Conflict of interest

The authors declare no conflict of interest.

[1] H. Huppertz, B. von der Eltz, *J. Am. Chem. Soc.* **2002**, *124*, 9376–9377.
[2] J. O. Edwards, V. Ross, *J. Inorg. Nucl. Chem.* **1960**, *15*, 329–337.
[3] C. L. Christ, *Am. Mineral.* **1960**, *45*, 334–340.
[4] O. Conrad, C. Jansen, B. Krebs, *Angew. Chem. Int. Ed.* **1998**, *37*, 3208–3218.
[5] H. Diercks, B. Krebs, *Angew. Chem.* **1977**, *89*, 327–328.
[6] B. Krebs, W. Hamann, *Z. Kristallogr.* **1983**, *162*, 149–150.
[7] J. Peters, B. Krebs, *Acta Crystallogr. Sect. B* **1982**, *38*, 1270–1272.
[8] A. Weiss, A. Weiss, *Z. Naturforsch. B* **1953**, *8*, 104.
[9] A. Weiss, A. Weiss, *Z. Anorg. Allg. Chem.* **1954**, *276*, 95–112.
[10] H. Emme, H. Huppertz, *Acta Crystallogr. Sect. C* **2005**, *61*, i29–i31.
[11] H. Emme, H. Huppertz, *Chem. Eur. J.* **2003**, *9*, 3623–3633.
[12] M. K. Schmitt, H. Huppertz, *Z. Naturforsch. Sect. B* **2017**, *72*, 977–982.
[13] J. S. Knyrim, F. Roessner, S. Jakob, D. Johrendt, I. Kinski, R. Glaum, H. Huppertz, *Angew. Chem. Int. Ed.* **2007**, *46*, 9097–9100; *Angew. Chem.* **2007**, *119*, 9256–9259.
[14] S. C. Neumair, R. Glaum, H. Huppertz, *Z. Naturforsch. Sect. B* **2009**, *64*, 883–890.
[15] S. C. Neumair, R. Kaindl, H. Huppertz, *Z. Naturforsch. Sect. B* **2010**, *65*, 1311–1317.
[16] S. C. Neumair, S. Vanicek, R. Kaindl, D. M. Többens, C. Martineau, F. Taulelle, J. Senker, H. Huppertz, *Eur. J. Inorg. Chem.* **2011**, 4147–4152.
[17] G. Sohr, D. M. Többens, J. Schmedt auf der Günne, H. Huppertz, *Chem. Eur. J.* **2014**, *20*, 17059–17067.
[18] Y. Wu, J.-Y. Yao, J.-X. Zhang, P.-Z. Fu, Y.-C. Wu, *Acta Crystallogr. Sect. E* **2010**, *66*, i45.
[19] S. Jin, G. Cai, W. Wang, M. He, S. Wang, X. Chen, *Angew. Chem. Int. Ed.* **2010**, *49*, 4967–4970; *Angew. Chem.* **2010**, *122*, 5087–5090.
[20] M. Mutailipu, M. Zhang, H. Li, X. Fan, Z. Yang, S. Jin, G. Wang, S. Pan, *Chem. Commun.* **2019**, *55*, 1295–1298.
[21] S. Han, C. Huang, A. Tudi, S. Hu, Z. Yang, S. Pan, *Chem. Eur. J.* **2019**, *25*, 11614–11619.
[22] I. H. Jen, Y.-C. Lee, C.-E. Tsai, K.-H. Lii, *Inorg. Chem.* **2019**, *58*, 4085–4088.
[23] C. Chen, B. Wu, A. Jiang, G. You, *Sci. Sin. Ser. B (Engl. Ed.)* **1985**, *28*, 235–243.
[24] C. Chen, Y. Wu, A. Jiang, B. Wu, G. You, R. Li, S. Lin, *J. Opt. Soc. Am. B* **1989**, *6*, 616–621.
[25] Y. Wu, T. Sasaki, S. Nakai, A. Yokotani, H. Tang, C. Chen, *Appl. Phys. Lett.* **1993**, *62*, 2614–2615.
[26] J.-M. Tu, D. A. Keszler, *Mater. Res. Bull.* **1995**, *30*, 209–215.
[27] Y. Mori, I. Kuroda, S. Nakajima, T. Sasaki, S. Nakai, *Appl. Phys. Lett.* **1995**, *67*, 1818–1820.
[28] M. Iwai, T. Kobayashi, H. Furuya, Y. Mori, T. Sasaki, *Jpn. J. Appl. Phys.* **1997**, *36*, L276–L279.
[29] L. Mei, Y. Wang, C. Chen, B. Wu, *J. Appl. Phys.* **1993**, *74*, 7014–7015.
[30] K. M. Ok, *Chem. Commun.* **2019**, *55*, 12737–12748.
[31] F. Liebau, *Structural Chemistry of Silicates: Structure, Bonding, and Classification*, Springer Science & Business Media, **2012**.
[32] H. Emme, C. Despotopoulou, H. Huppertz, *Z. Anorg. Allg. Chem.* **2004**, *630*, 2450–2457.
[33] G. Heymann, T. Soltner, H. Huppertz, *Solid State Sci.* **2006**, *8*, 821–829.
[34] M. Glätzle, G. J. Hoerder, H. Huppertz, *Z. Naturforsch. Sect. B* **2016**, *71*, 535–542.
[35] I. D. Brown, D. Altermatt, *Acta Crystallogr. Sect. B* **1985**, *41*, 244–247.
[36] N. E. Brese, M. O'Keeffe, *Acta Crystallogr. Sect. B* **1991**, *47*, 192–197.
[37] R. Hoppe, S. Voigt, H. Glaum, J. Kissel, H. P. Müller, K. Bernet, *J. Less-Common Met.* **1989**, *156*, 105–122.
[38] B. B. Zhang, G. Q. Shi, Z. H. Yang, F. F. Zhang, S. L. Pan, *Angew. Chem. Int. Ed.* **2017**, *56*, 3916–3919; *Angew. Chem.* **2017**, *129*, 3974–3977.
[39] B. H. Lei, Z. H. Yang, S. L. Pan, *Chem. Commun.* **2017**, *53*, 2818–2821.
[40] J. P. Laperches, P. Tarte, *Spectrochim. Acta* **1966**, *22*, 1201–1210.
[41] G. Blasse, G. P. M. van de Heuvel, *Phys. Status Solidi A* **1973**, *19*, 111–117.
[42] R. Kaindl, G. Sohr, H. Huppertz, *Spectrochim. Acta Part A* **2013**, *116*, 408–417.
[43] A. Haberer, R. Kaindl, O. Oeckler, H. Huppertz, *J. Solid State Chem.* **2010**, *183*, 1970–1979.
[44] S. K. Kurtz, T. T. Perry, *J. Appl. Phys.* **1968**, *39*, 3798–3813.
[45] D. A. Roberts, *IEEE J. Quantum Electron.* **1992**, *28*, 2057–2074.
[46] K. J. D. Mackenzie, M. E. Smith, *Multinuclear solid-state NMR of inorganic materials, Vol. 1*, Elsevier Science Ltd., Kidlington, Oxford, UK, **2002**.
[47] D. Walker, M. A. Carpenter, C. M. Hitch, *Am. Mineral.* **1990**, *75*, 1020–1028.
[48] D. Walker, *Am. Mineral.* **1991**, *76*, 1092–1100.
[49] H. Huppertz, *Z. Kristallogr.* **2004**, *219*, 330–338.
[50] G. M. Sheldrick, Bruker AXS Inc., Madison, Wisconsin, USA, **2001**.
[51] G. M. Sheldrick, *Acta Crystallogr. Sect. A* **2008**, *64*, 112–122.
[52] G. M. Sheldrick, *Acta Crystallogr. Sect. C* **2015**, *71*, 3–8.
[53] L. J. Farrugia, *J. Appl. Crystallogr.* **2012**, *45*, 849–854.
[54] A. L. Spek, *Acta Crystallogr. Sect. D* **2009**, *65*, 148–155.
[55] L. M. Gelato, E. Parthé, *J. Appl. Crystallogr.* **1987**, *20*, 139–143.
[56] S. J. Clark, M. Segall, C. J. Pickard, P. Hasnip, M. Probert, K. Refson, M. C. Payne, *Z. Kristallogr.* **2005**, *220*, 567–570.
[57] A. Rappe, K. Rabe, E. Kaxiras, J. D. Joannopoulos, *Phys. Rev. B* **1990**, *41*, 1227–1230.
[58] J. P. Perdew, K. Burke, M. Ernzerhof, *Phys. Rev. Lett.* **1996**, *77*, 3865–3868.
[59] C. Aversa, J. E. Sipe, *Phys. Rev. B* **1995**, *52*, 14636–14645.
[60] B. B. Zhang, M. H. Lee, Z. H. Yang, Q. Jing, S. L. Pan, M. Zhang, H. P. Wu, X. Su, C. S. Li, *Appl. Phys. Lett.* **2015**, *106*, 031906.
[61] C. G. Broyden, *IMA J. Appl. Math.* **1970**, *6*, 76–90.
[62] R. Fletcher, *Comput. J.* **1970**, *13*, 317–322.
[63] D. Goldfarb, *Math. Comp.* **1970**, *24*, 23–26.
[64] D. F. Shanno, *Math. Comp.* **1970**, *24*, 647–656.
[65] H. J. Monkhorst, J. D. Pack, *Phys. Rev. B* **1976**, *13*, 5188–5192.
[66] C. J. Pickard, F. Mauri, *Phys. Rev. B* **2001**, *63*, 245101.
[67] Bruker, Billerica, MA, **2008**.
[68] Horiba Jobin Yvon GmbH, Bensheim, **2005**.

[69] L. Bayarjargal, B. Winkler, E. Haussühl, R. Boehler, *Appl. Phys. Lett.* **2009**, *95*, 061907.

[70] J. W. E. Weiss, D. L. Bryce, *J. Phys. Chem. A* **2010**, *114*, 5119–5131.

[71] S. Cavadini, A. Lupulescu, S. Antonijevic, G. Bodenhausen, *J. Am. Chem. Soc.* **2006**, *128*, 7706–7707.

[72] Z. Gan, *J. Am. Chem. Soc.* **2006**, *128*, 6040–6041.

[73] A. Brinkmann, A. P. M. Kentgens, *J. Am. Chem. Soc.* **2006**, *128*, 14758–14759.

[74] M. H. Levitt, in *Encyclopedia of Nuclear Magnetic Resonance. Volume 9, Advances in NMR* (Eds.: D. M. Grant, R. K. Harris), Wiley, **2002**, pp. 165–196.